21.4 CONTAINMENT AND BIMAC-DEVICE PERFORMANCE AGAINST EX-VESSEL STEAM EXPLOSIONS (EVE)

21.4.1 Overall considerations

Ex-Vessel Steam Explosions are energetic fuel-coolant interactions that are triggered from melt-coolant mixtures that are developed as the melt released from the RPV falls into, and traverses the depth of a water pool below. Metallic melts such as those expected here for low pressure scenarios are especially prone to such energetic behavior. The result is pressure pulses that may reach the kbar range. They are not quite sufficient to generate self-sharpening shock waves in water, but are potentially capable, when large quantities of melt are involved together with highly subcooled water, of loading major structures to failure. Failure is characterized by the impulse—the time-integral of the pressure acting on the surface of the structure (see Subsection 21.4.4.4).

While in-vessel explosions (IVE) are essentially of exclusive interest to PWRs, ex-vessel explosions (EVE) are of primary interest to BWRs. One reason is that in BWRs the initial release can be mostly metallic. Another reason is that LDW designs have traditionally employed very large-height geometries, which, when flooded, form deep water pools below the reactor vessel. Still another reason is that in BWRs the structural damage of the reactor pedestal can be much more serious to containment integrity than that of reactor cavities in PWRs.

From another perspective, these large geometries in BWRs have been thought of as a means to assuring long-term coolability for core-on-the-floor scenarios. The idea in this case is that deep flooding would provide sufficient travel distance for the melt to fragment and quench, thus forming a coolable debris bed on the LDW floor. Currently the Swedish-built BWRs operate under this premise. However, the efficacy of this coolability concept can be questioned, while at the same time the thus-generated threat to the structural integrity of the reactor pedestal has been raised (Theofanous et al, 1995, Almström et al, 1999).

In the ABWR SSAR (1994), while the term “steam explosion” is used, the actual calculations only reflect a mild steam spike with a peak pressure of 1 MPa (145 psi). For the SBWR on the other hand, the EVE threat was appreciated, and a massive obstacle, the “corium shield” (a 4-inch-thick (0.1 m) cylindrical steel piece surrounding the open LDW space), was incorporated to protect the reactor pedestal from such explosive loads. Such a shield is not necessary in the ESBWR design.

In the ESBWR, besides the pedestal we also need to be concerned about the “worthiness” of the BiMAC structure against such explosive events. We will show that this too can be build to withstand major explosive events, as is the pedestal. However, given the uncertainties involved in mode of RPV failure, and in the simulation of 3D melt-water mixing and explosion in large geometries (deep, sub-cooled water pools in particular), we will not attempt to demonstrate that failure is physically unreasonable under all conceivable scenarios. Rather our management approach is based on limiting such scenarios so that at most we have to deal with shallow, saturated water pools. This turned out to be possible because of the simple design of the primary coolant system, and it was achieved by means of containment layout changes as described in the next section.

The simple idea is that there can be no explosions in the absence of water, and it is possible to show that this can be achieved in 99% [74%] of the Class I (that is LP) sequences. Water needs to be added to the LDW soon after the first ex-vessel melt relocation, this is done by means of a deluge system, and a complementary aspect of this approach is ensuring that this does not occur prematurely. As explained in detail in Subsection 21.5, a maximum unreliability of this LDW deluge system was placed at 0.1%.

This basic approach to the EVE threat is further buttressed by three additional elements:

a. Reiterating analyses that show shallow, saturated water pools to yield highly voided premixtures that resist triggering and escalation to detonation,

b. Showing that the pedestal can stand very strong energetic events involving melt pour rates of up to ~1 metric tons/s (1.1 ton/s) into sub-cooled water pools of depths up to 5 m (16 ft),

c. Showing that the BiMAC can withstand perhaps not all, but a significant fraction of such arbitrarily severe conditions (relative to the cases of interest).

In regards to item (a), the basic ideas have been expressed previously by Henry and Fauske, 1981, Theofanous et al., 1987, and were further confirmed by others, including all experimental evidence available to-date. In regards to item (b), the basic idea is explosion venting as articulated and shown by the results in the first consideration of explosive load delivery in open pool systems (Yuen and Theofanous, 1995). Venting is an effect that produces a smaller impulse to distant structures by reducing both the time for the pressure wave unloading at the pool surface, as well as the amplitude of the wave that propagates radially outwards.

The technology used in our assessment is based mostly on work done under DOE's ARSAP program, as summarized in Subsection 21.4.3, and on some follow up work done for the US NRC in the 1998-2003 time frame.

21.4.2 ESBWR Design

Regarding potential damage from EVEs, the relevant structures are the reactor pedestal, a 2.5 m (8.2 ft) reinforced concrete wall as illustrated in Figure 21.4.2-1, and the BiMAC device, a layer of thick-walled steel pipes that are well embedded into reinforced concrete in a way that they are supported in all directions as shown in Figure 21.4.2-2. The structural details of both are given in Subsection 21.4.4.4.

Failure of the reactor pedestal, along with the steel liner on it, would constitute violation of the containment boundary. While the load-bearing capacity of this structure is 2.85 MPa (413 psi), explosive-level pressures acting on a millisecond time scales can produce sufficient extent of concrete cracking, along with liner stretching and tearing, to compromise leak-tightness of the containment. Failure of the BiMAC device on the other hand is defined as crushing (or locally collapsing) of the pipes so that they cannot perform their heat removal function — channeling the so-generated two-phase mixture from the bottom onto the top of the debris mass. Such failure would raise the possibility of continuing corium-concrete interactions, basemat penetration, and containment pressurization by the so-generated non-condensable gases.

As noted already, the principal element of our approach on EVE is to address the quantities (and subcooling) of water in the LDW, just prior to melt exiting the RPV. It is at this time that the relocation can be potentially massive, and thus of energetic concern. In particular:

a. As a result of our early interactions with Level-1 PRA personnel and the ESBWR designers, modifications in the containment layout were made so as to prevent subcooled water, from entering the LDW through the UDW; in particular this covered the re-routing of GDCS overflow, and to prevent overflow of the suppression pool water to the LDW;

b. A BiMAC device activation system was defined (see Subsection 21.5) by integrating environmental signals (high temperatures) with valving action on the LDW deluge lines (feeding off the GDCS pools) so that premature flooding is to be reliably prevented.

Item (b), as discussed in Chapter 21.5 (on BMP), is based on a BiMAC design that makes it function immediately upon opening up the deluge lines. Thus there is no need to pre-flood the LDW.

In regards to building in additional margins, and with the pedestal already designed quite robustly to satisfy other structural considerations (load-bearing capacity under seismic conditions), our considerations focused on having a structurally robust BiMAC as well. As the structural response calculations in Subsection 21.4.4.4 show this was achieved to a significant degree by the choice of pipe diameter and wall thickness, and the embedded mutually supporting configuration.

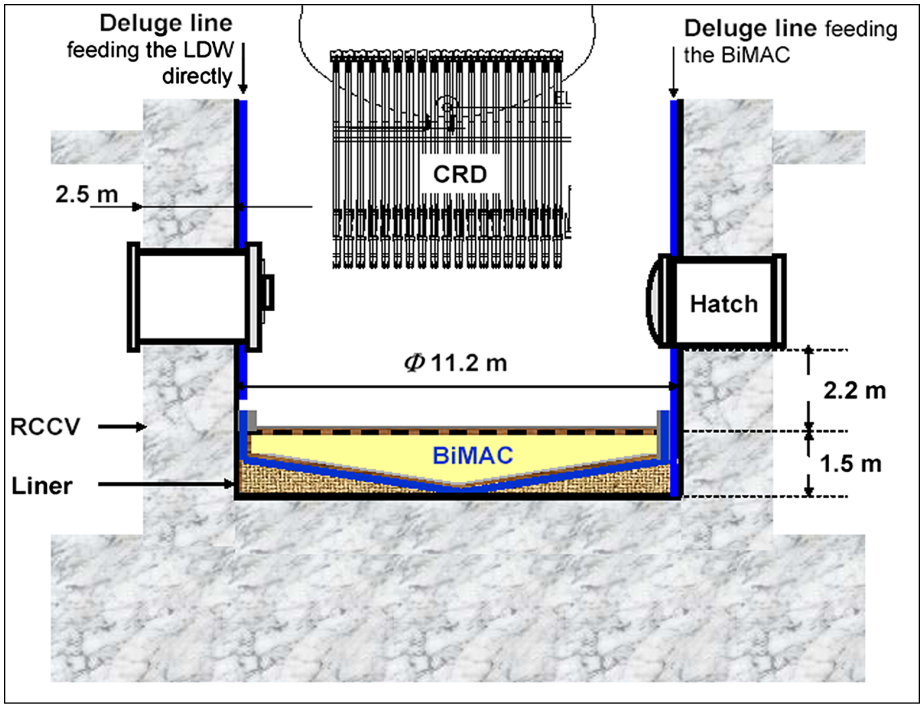

Figure 21.4.2-1. The Overall Ldw Geometry Relevant to EVEs

The overall LDW geometry relevant to EVEs, including the structural composition, and steel liner.

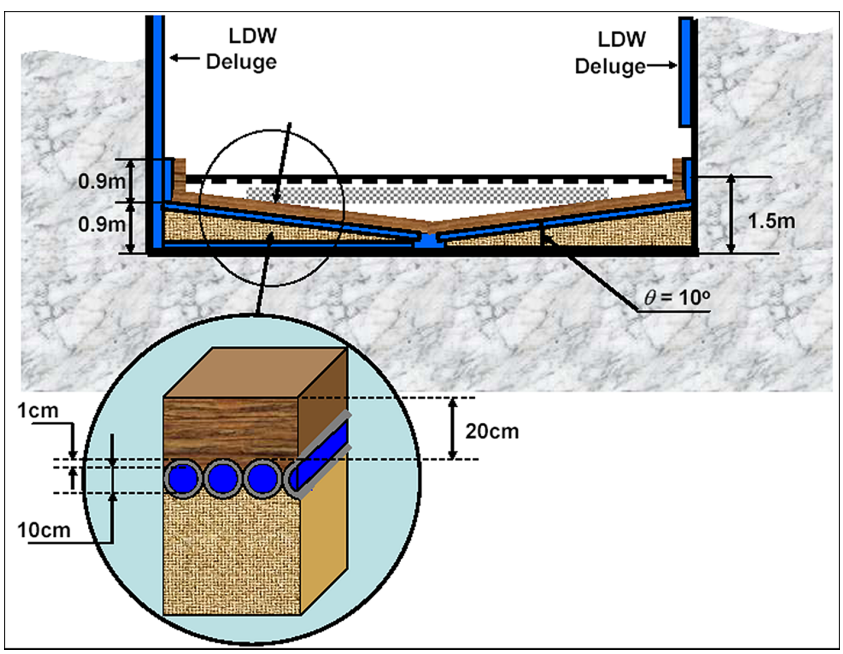

Figure 21.4.2-2. BiMAC device geometry in pedestal region.

The BiMAC device in the pedestal region, and key dimensions of the geometry. The pipes are 10 cm in diameter (4 inches) and 1 cm thick (schedule 80). The inset shows detail arrangement of BiMAC pipes embedded within the concrete, with a

0.2 m thick refractory layer on top. Final design details of the BiMAC will be consistent with Reference 21.5-40.

21.4.3 Previous Work

The Steam Explosions Review Group (SERG) convened by the US NRC, in both of its meetings, focused on the alpha mode containment failure (SERG-1, 1985; SERG-2, 1995)—an energetic steam explosion in the lower plenum of the RPV, leading to the generation of internal and then external missiles that penetrate the containment shell. Thus only in-vessel steam explosions for PWRs were considered in detail. For BWRs, the lower plenum design, largely and densely occupied by control rod guide tubes, was considered to be generically prohibitive of the large scale events required for α-failure. Other licensing-related work for in-vessel steam explosions is the ROAAM-based consideration of α-failure in Sizewell B (Turland et al, 1994) and of lower head integrity for the AP600 (Theofanous et al, 1999c).

Major milestones in understanding the physics of steam explosions, and in the development of computational and modeling technology for simulating energetics, have been summarized previously by Theofanous et al (1987), Amarasooriya and Theofanous (1991), Theofanous et al (1994, 1995), Fletcher and Theofanous (1997), Theofanous and Yuen (1995), and Theofanous et al (1999abc). The key idea in modeling energetics is that of "microinteractions" (Yuen and Theofanous, 1999). The computer codes PM-ALPHA (Yuen and Theofanous, 1995) and ESPROSE.m (Yuen and Theofanous, 1995), for premixing and propagation respectively, are still the state-of-the-art (CFD simulation) tools. Verification and validation of these codes (Theofanous et al, 1999a, Theofanous et al, 1999b) has been documented and reviewed extensively (full ROAAM review) during the AP600 Design Certification effort. These codes are now also used by US NRC consultants during licensing reviews such as for ex-vessel explosions in the AP1000 (Westinghouse, 2002, Khatib-Rabar and Ismaeli, 2005).

There is no previous work on fragility to impulsive loads of a structure such as the BiMAC. Previous assessments of thick reinforced concrete walls, done only in a very crude manner (Rashid, Theofanous, and Foadian, 1995), indicates that an impulse magnitude of ~100 kPa.s (14.5 psi.s) could begin to inflict significant damage (cracking) on a reinforced concrete wall (pedestal) that is 1.5 m (4.9 ft) thick. At such levels of explosion impulse, cracking was found to be significantly reduced for a 7,000 psi (48 MPa) concrete, and to be virtually eliminated for a 10,000 psi (69 MPa) concrete. However, such improved grades of concrete are more expensive than the "normal" 5,000 psi (34 MPa) grade considered for ESBWR.

We note in passing that the pedestal fragility in the ABWR safety analysis (ABWR SSAR, GE, 1994) was (stated to be) based on an approach similar to that applied for the Grand Gulf Mark III assessment of NUREG-1150 (1990) — an approach based on energy absorption of a 6 cm-thick (2.4 in) liner, that produced a failure impulse of 24 kPa.s (3.5 psi.s). The ABWR result was expressed in terms of a peak pressure of "at least 0.85 MPa" (123 psi), this was then translated to a steam explosion involving 9.5% of the ABWR core (~22 metric tons, 24 tons), and on this basis it was concluded that "This failure mechanism need not be considered further in the containment event trees or the uncertainty analysis."

21.4.4 Present Assessment

21.4.4.1 Key Physics

In an open system, such as the LDW of the ESBWR, the susceptibility of a pre-mixture to triggering decreases as the volume fraction of steam (the void fraction) in it increases; thus subcooled water pools are considerably more prone to energetic behavior in comparison to saturated pools. On the other hand, the energetics of an explosion increases along with the total quantity of melt found in the pre-mixture at the time of triggering; thus explosions in deep pools can be more damaging in comparison to those in shallow pools. Both of these features, the subcooling and the depth, couple with a host of other parameters (melt mass break-up, momentum exchanges between melt and coolant, phase changes of coolant, etc) in a highly dynamic set of phenomena, to produce, for any particular mixing realization, an evolution of pre-mixtures, each one with a particular susceptibility to triggering and efficiency in thermal-to-mechanical energy conversion. As in our previous assessments done for licensing purposes (Theofanous et al, 1999c), both triggering and efficiency are treated here in a bounding fashion; that is, triggering is assumed to occur at the time of most favorable (least voided) premixture, and key limitations to energetics, such as fuel freezing during premixing, and non-equilibrium in the micro-interactions are not accounted for. So, in assessing EVE loads, we rely on well-qualified mechanisms and tools to account for pressure wave unloading/venting phenomena applied to idealized/efficient (to the extent that the Thermodynamics allow; this is where premixture voiding comes into play) explosions.

Current understanding of structural integrity under impulsive loading derives from work with high explosives (HE), acting mostly within a gaseous medium. In comparison to these explosions, in EVEs the pressure pulses would be of much lower amplitudes and of a much longer duration. Still, with a structure whose inverse natural frequency is much longer than the pulse width, it is the delivered impulse that characterizes damage, and existing HE-derived tools, such as the DYNA3D code used in this work (Noble et al, 2005), can be expected to be well applicable. Again conservatively, in this application, we ignore the dissipative effects (and so-reduced actual loading) due to fluid-structure interaction. That is, pressure pulses obtained from explosion calculations carried out in a rigid wall geometry, are then applied to the structural calculation.

As concrete is highly resistant to compression but rather weak in tension, the mode of failure for the reactor pedestal is concrete cracking, separation from the rebar net, spallation at the "free end" and rebar-yielding that result in displacements sufficient to both, begin to lose load-bearing capacity as well as strain the liner to failure. In other words, to lose containment integrity, both the liner must be strained to failure (typically ~30% effective plastic strain) and the wall must be damaged enough to not be able to support leak tightness. Reinforcement, sometimes pre-tensioned, is employed to balance load-bearing performance in this respect. However, at the kbar range of pressures of interest here, this load bearing is to reduce the extent, rather then eliminate cracking, and in any case it is not considered in this assessment. For the BiMAC, the same mechanisms are superposed to yield deformation of the steel pipes, and eventually plastic yielding that when it is of sufficient extent leads to collapse, and thus failure of BiMAC function.

21.4.4.2 Probabilistic Framework

According to our emphasis in eliminating melt-down sequences that involve deep, subcooled water pools in the LDW, our quantification approach is largely based on the Integrated ROAAM; that is, accounting for aspects of the design that prohibit such large-scale contact scenarios. In this task our work has interacted with Level I PRA and in the end it has been informed by the results obtained thereby. The rest of our task is to demonstrate some significant margins, both for the Pedestal and the BiMAC, even in many scenarios that are postulated to not meet the criteria of "shallow, saturated pools", and this will be done rather roughly, as we feel this is consistent with the demonstration needs in this case.

In treating the EVE threat we need only consider Class I accidents. They amount to ~90% [~65%] of the CDF, and of these the proportions with High (H>1.5 m (4.9 ft)), Medium (0.7<H<1.5 (2.3 ft<H<4.9ft)), and Low (H<0.7 (2.3 ft)) water pool depths (on the LDW floor, at the time of vessel breach) are 0.9% [10%], 0.1% [16%], and 99% [74%] respectively. Adjusting these proportions for the 0.6% [16%] of the Class IV accidents that revert to Class I with Low water pool levels [99.5%] is not significant. This in combination with the extremely low CDF, satisfies the Integrated ROAAM criteria for ignoring scenarios that are remote and speculative.

The 1.5 m (4.9 ft) demarcation for the "deep" water pool was selected in consideration of the position of the hatch door, combined with a collective judgment in which we aimed to leave out ranges of conditions that we do not feel could be reasonably captured by current capabilities and experience. On the other hand it should be noted that this choice is not critical to our conclusions—we found that those rare sequences that exceed the low height category (H<0.7 m (2.3 ft)) tend to produce fully-flooded LDW conditions (which are also subcooled), while the low level category results from condensation processes thus yielding saturated pools.

As noted above saturated premixtures become highly voided, and are highly resistant to supporting the escalation of spontaneous triggers towards detonations. Moreover, even if any explosions were to be developed, they would be rather inefficient, and of low energetics. One task in the next section is to illustrate this behavior for shallow/saturated pools. Our other task is to contrast this behavior with that of subcooled/deep pools, and provide some perspectives on the level of energetics that could possibly result in the latter case. This then together with the perspectives on structural failure provided in Subsection 21.3.4.4 will yield an understanding of the resilience of these structures to hypothetical energetic events from EVEs.

21.4.4.3 Quantification of Loads

Steam explosion calculations were carried out with the PM-ALPHA.L-3D, and ESPROSE.m codes for water pool depths of 1, 2 and 5 m (3, 6.5 and 16 ft) with 100 K (180 °F) subcooling. The 2 m (6.5 ft) deep case was also considered with saturated water. In all cases the pour rate was set at 720 kg/s (1600 lbm/s), which was based on a penetration failure and gravity draining aided by 0.2 MPa (29 psi) overpressure. In the premixing calculation the melt enters the domain over an area of ~0.03 m^2 (0.3 ft^2), with a velocity of 13 m/s (43 ft/s), and a volume fraction of 22%.

The premixing calculations were run in 3D, while for the explosion, in order to capture the wave dynamics at a sufficient resolution, the calculations were run in 2D axi-symmetric geometry. Grid-convergence studies were made to confirm that this is indeed the case. The proximity of

the explosion to the sidewall (off-center pours) was investigated by using domains of 4 m (13 ft) in diameter. The positions for which dynamic loads are given are summarized in Figure 21.4.4.3-1.

All parameters in these computations were selected in a conservative fashion, and consistently with experience from previous such assessments (i.e., Theofanous et al, 1996). In particular, for the key explosion parameters β and γ (β is the fragmentation model parameter, and γ is the thermal enhancement factor that is used to account for the effect of pressure on microinteractions) we have used values of 9 and 4-2-1 (that is, a value reducing from 4 to 2 to 1 as local pressures increase from ambient to 1 kbar (14,500 psi)), consistently with the interpretation of the highly energetic KROTOS tests (Theofanous et al, 1999b).

The premixing results are summarized in Figures 21.4.4.3-2a to 21.4.4.3-2d. In all cases there is the characteristic opening up due to the initial plunging (see also Appendix C), however the subsequent evolutions are quite different between the saturated and subcooled cases. In particular in (a) we see that at t=0.48 s there is an attempt to collapse, however further boiling leads to arrest and further expansion, while in all subcooled cases we see that this closing is actually completed to significant degree, thus leading to potentially energetic premixtures. Moreover we note that the collapse itself could provide the trigger needed to produce an explosion precisely at this opportune, from a premixing standpoint, time. One-to-one comparison is given in Figure 21.4.4.3-2d to further illustrate the differences in voiding patterns.

As expected the highly voided premixtures in the saturated pool case could not be made to escalate even with rather energetic triggers. All other cases produced explosions, and the results are summarized in Figures 21.4.4.3-3a to 21.4.4.3-3d in terms of the pressure transients and the resulting impulses on the bottom and the sidewalls. We can see that with one exception typical primary impulses on the bottom are ~100 kPa s (14.5 psi.s), while on the side they increase with pool depth from ~40 to 150 kPa s (6 to 22 psi.s). Also we can see the effect of venting, as in the deeper pools there is a second pulse due to side wall reflections that remain strong. These second pulses are of course not relevant to the open geometry of the LDW for pool depths of 1 or 2 meters (3 or 6.5 ft).

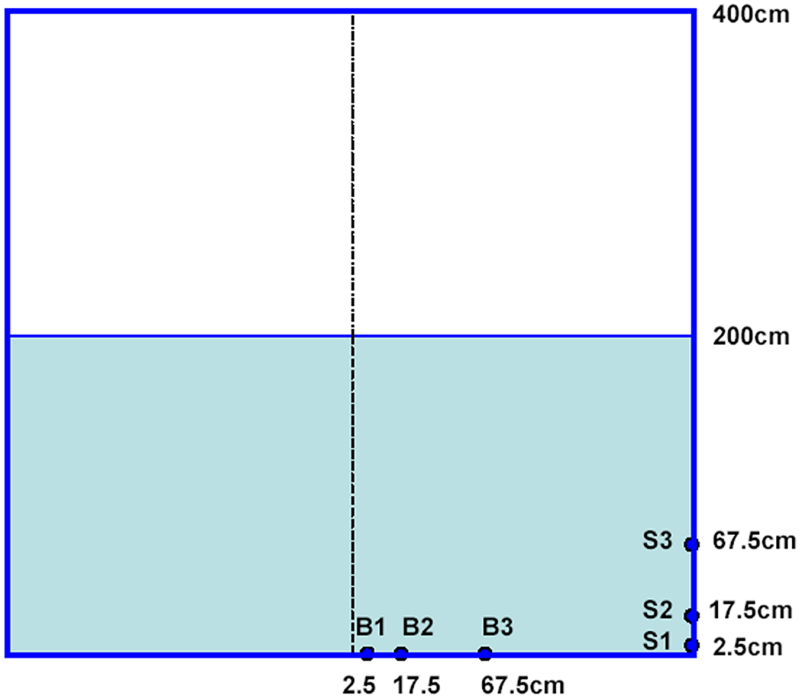

Figure 21.4.4.3-1. Cylindrical Cavity Model Used in the ESPROSE.m Calculation

The computational domain of a cylindrical cavity utilized in the ESPROSE.m calculation for the 2 m deep water pool case. B1, B2 and B3 are locations on bottom wall (basemat) and S1, S2 and S3 are locations on the sidewall (pedestal), where pressures and impulses are provided in subsequent figures. These locations remain the same for all pool dimensions considered.

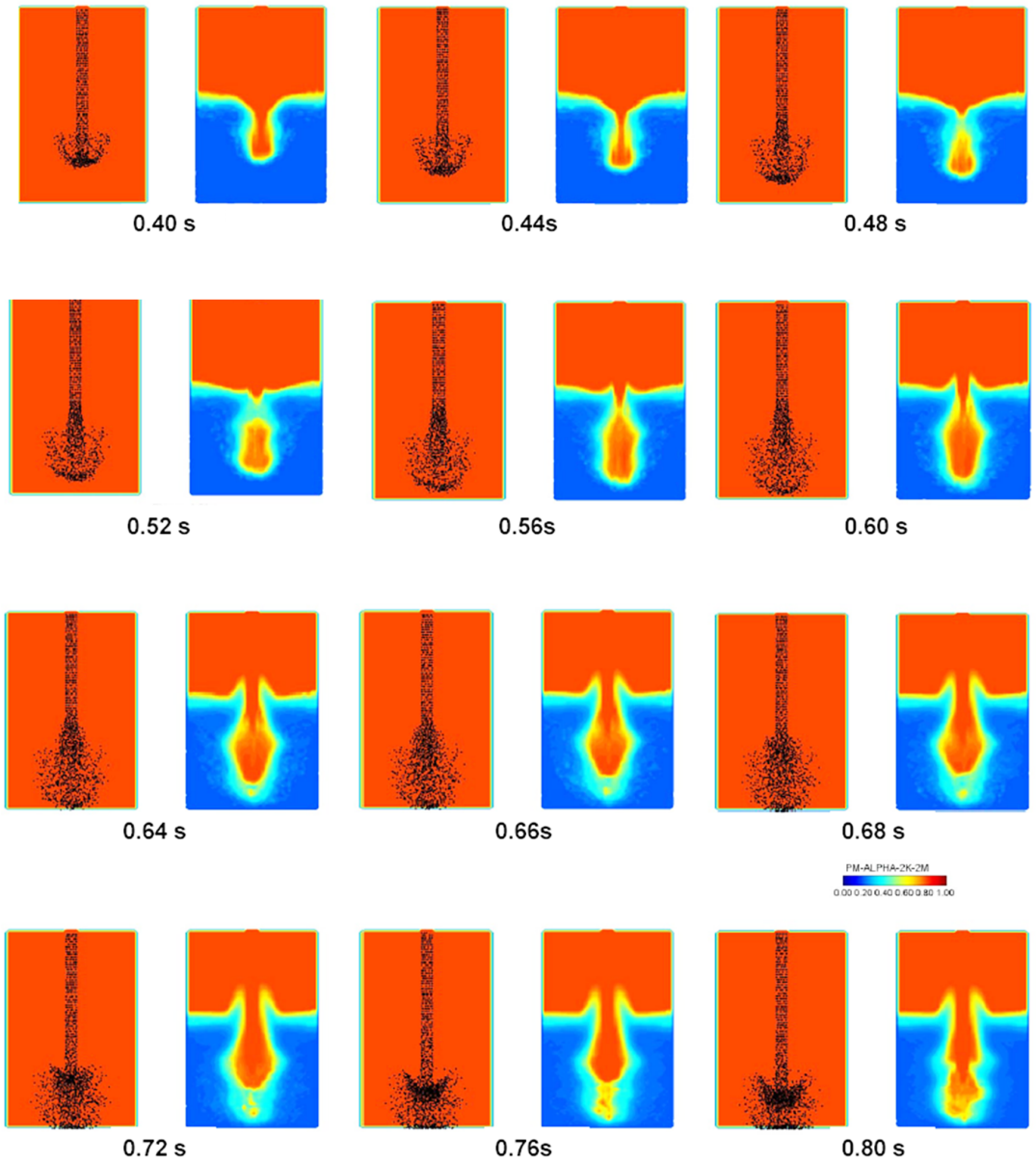

Figure 21.4.4.3-2a. Premixtures Evolution in a 2-Meter-Deep Pool, 2 K subcooling

Evolution of premixtures in a 2-meter-deep pool, 2 K subcooling. Melt (left) and void fraction (right) distributions.

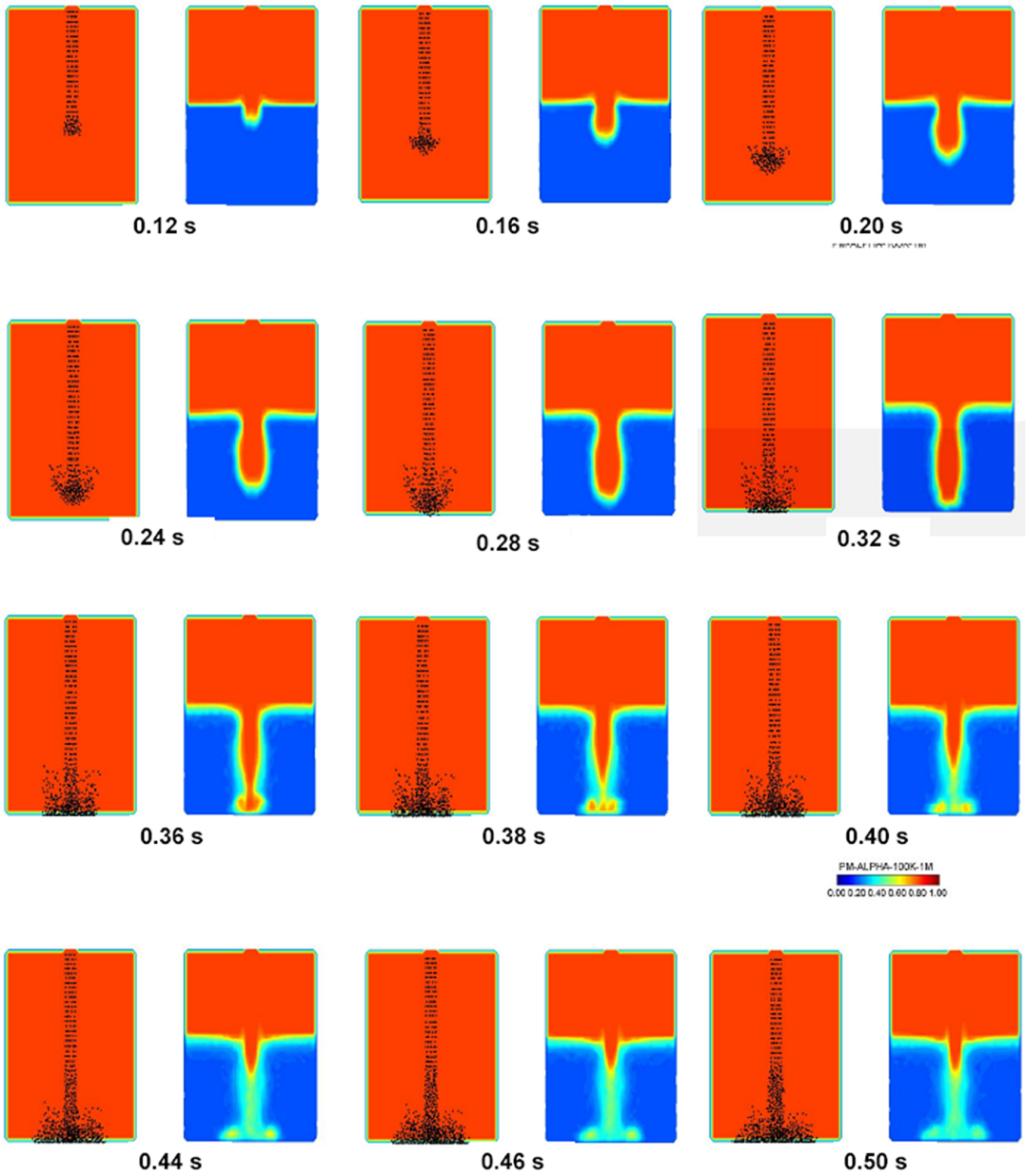

Figure 21.4.4.3-2b. Premixtures Evolution in a 1m-Deep Pool, 100 K Subcooling

Evolution of premixtures in a 1m-deep pool, with 100 K subcooling. Melt (left) and void fraction (right) distributions.

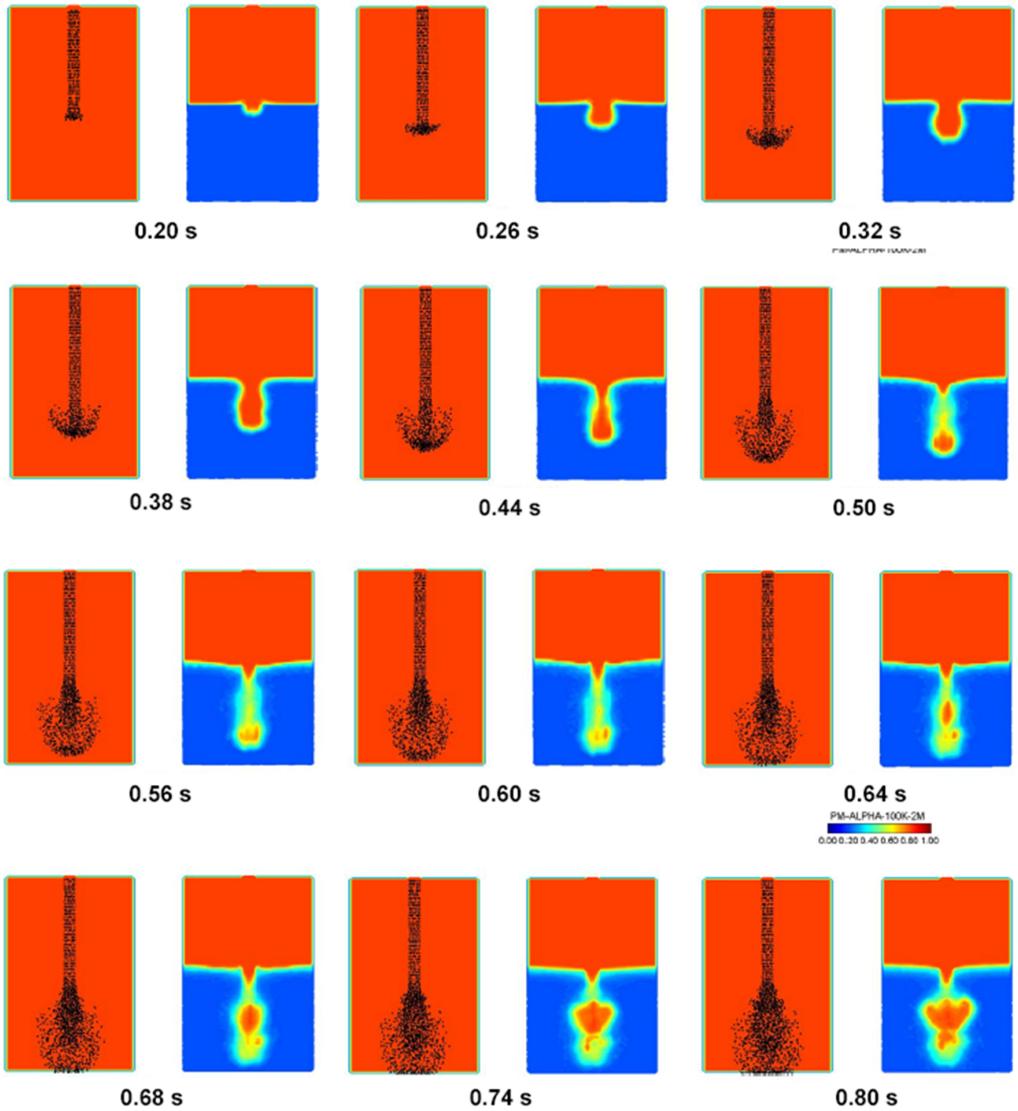

Figure 21.4.4.3-2c. Premixtures Evolution in 2-Meter-Deep Pool, 100 K Subcooling

Evolution of premixtures in a 2-meter-deep pool, with 100 K subcooling. Melt (left) and void fraction (right) distribution.

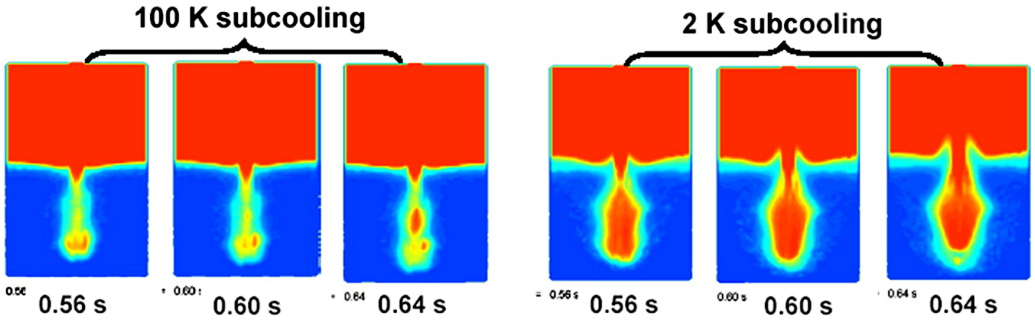

Figure 21.4.4.3-2d. Comparison of Premixing Patterns in 2m-Deep Pools

Comparison of premixing patterns in 2m-deep pools, with 100K and 2 K subcooling.

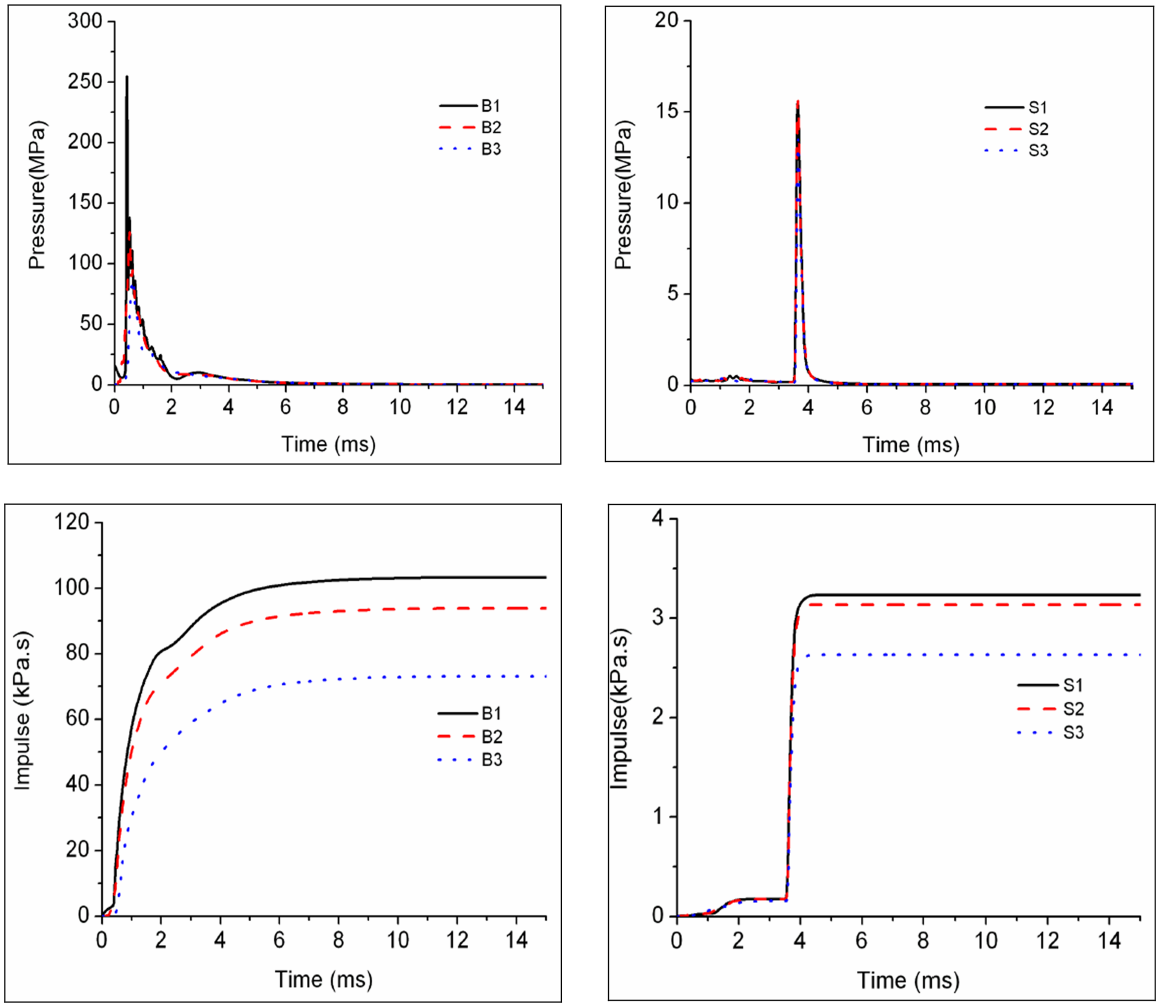

Figure 21.4.4.3-3a. Pressures and Impulses on the Floor (B) and Pedestal (S)

Pressures and impulses on the floor (B) and pedestal (S) from an explosion in 1 m deep, subcooled pool. Trigger time: 0.28s. The resulting impulse on the pedestal is insignificant, due to the effect of explosion venting.

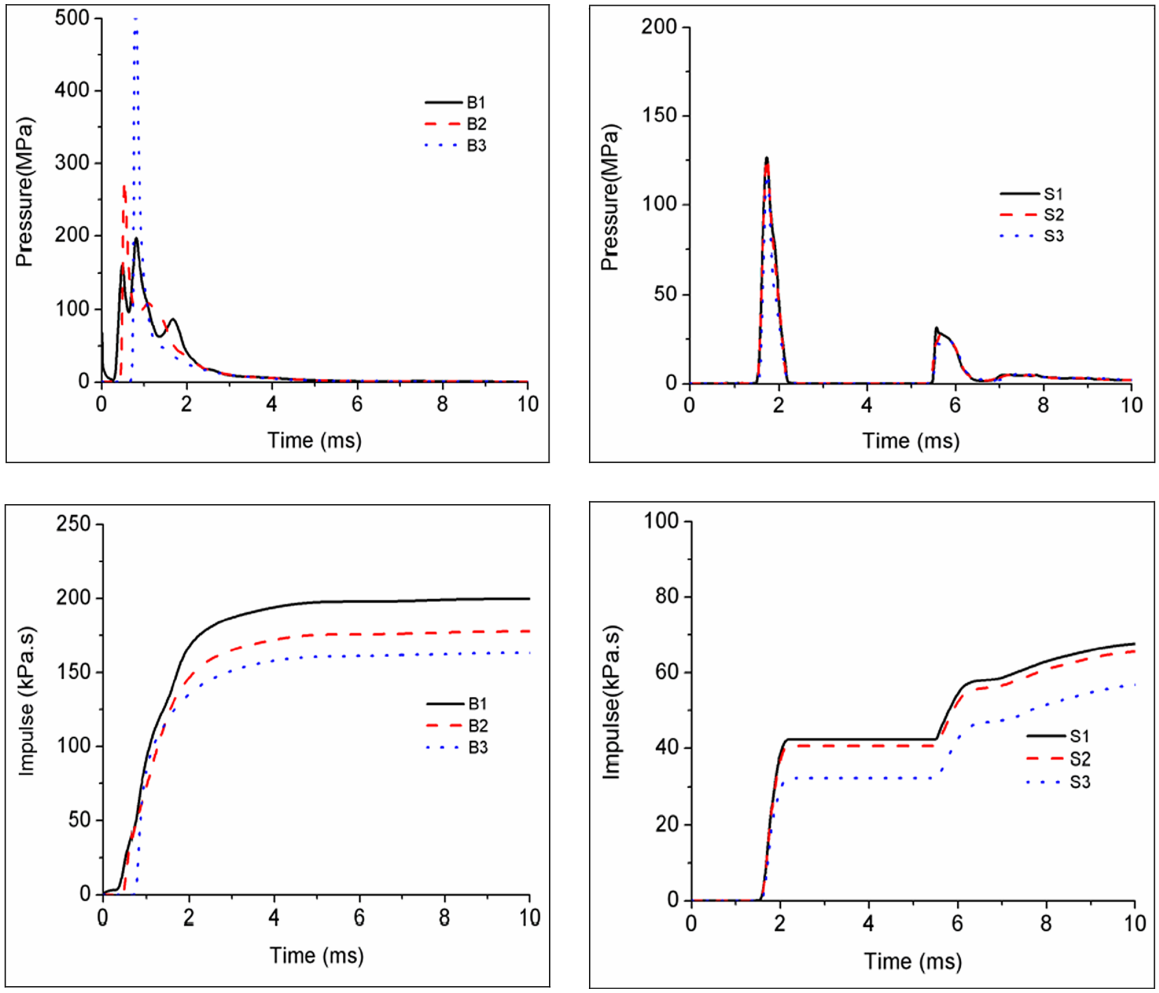

Figure 21.4.4.3-3b. Pressures and Impulses on the Floor (B) and Pedestal (S)

Pressures and impulses on the floor (B) and pedestal (S) from an explosion in 1 m deep, subcooled pool. Trigger time: 0.47s. No explosion developed when trigger energy of 20 kJ was used. A higher trigger energy (50 kJ) was needed for explosion to develop.

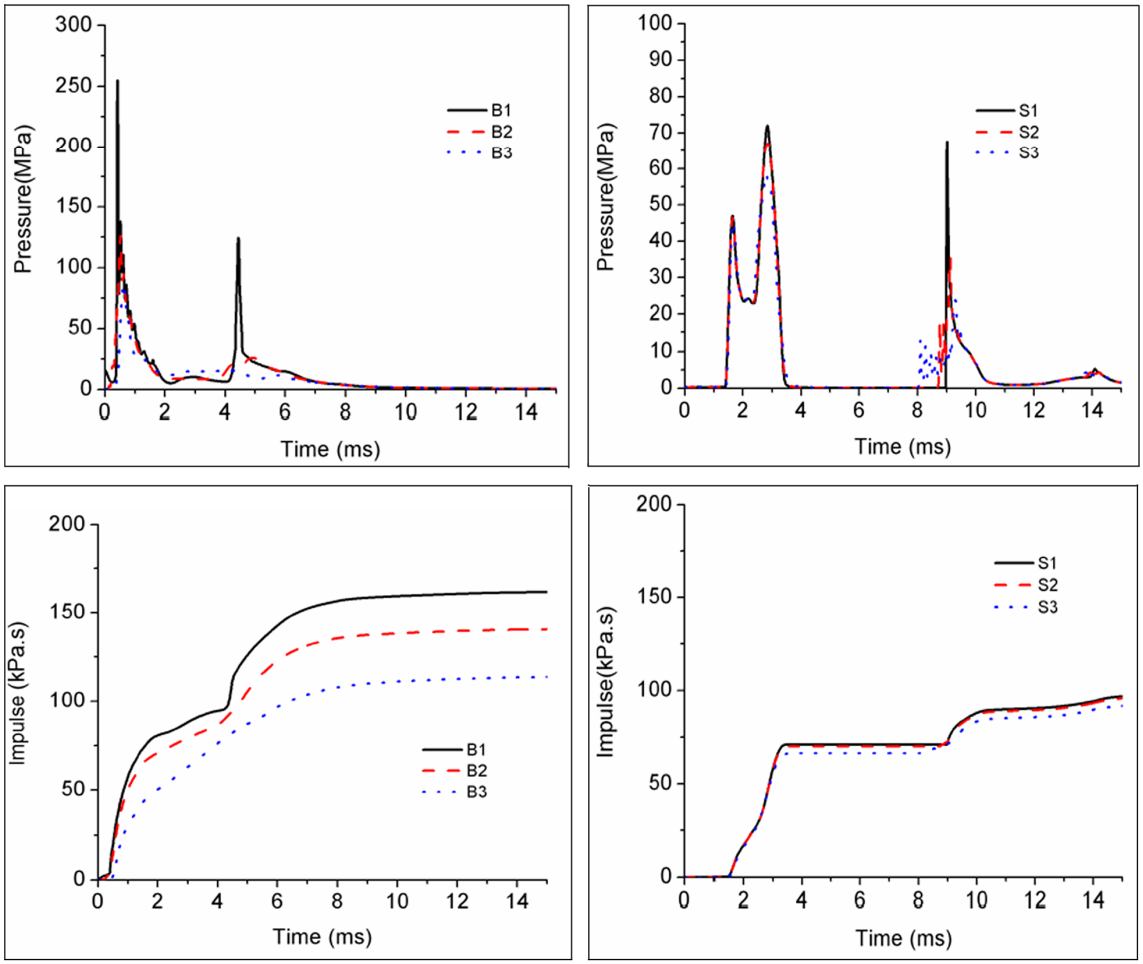

Figure 21.4.4.3-3c. Pressures and Impulses on the Floor (B) and Pedestal (S)

Pressures and impulses on the floor (B) and pedestal (S) from an explosion in 2 m deep, subcooled pool. Trigger time: 0.63s. Trigger energy was 20 kJ. The second pressure pulse is from the convergence of reflections off the side walls, and would not be present in an open LDW pool, even if the explosion were 2 m away from a side wall.

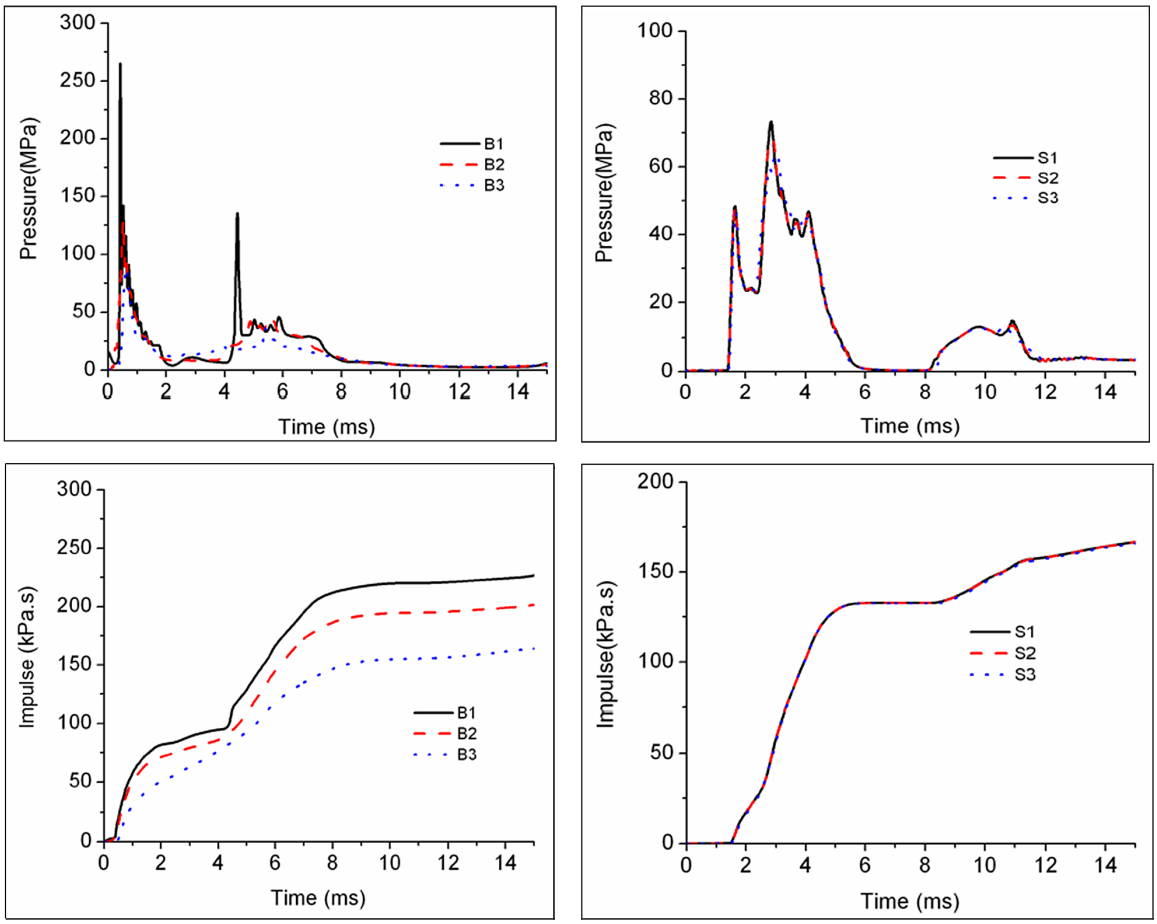

Figure 21.4.4.3-3d. Pressures and Impulses on the Floor (B) and Pedestal (S)

Pressures and impulses on the floor (B) and pedestal (S) from an explosion in 5 m deep, subcooled pool. Trigger time: 0.63s. Same remark on reflected wave convergence applies to the second pulse as in previous figure, although the larger inertia constraint here would still support some of this type of reflection even in 10 m in diameter pool.

21.4.4.4 Quantification of Fragility

The detailed structural makeup of the pedestal is shown in Figure 21.4.4.4-1. It was assumed that a standard, 5,000 psi (34 MPa) concrete mix will be used. This rebar-concrete material assembly, including the liner, was represented by the DYNA3D model shown in Figure 21.4.4.4-2 (DYNA3D Manual). Further details on the concrete model, the so-called K&C model (Karagozian and Case) can be found in Malvar et al (1997), and verification/validation of DYNA3D performance on problems of this type has just been released (Noble et al, 2005).

Calculations were carried out both with and without the 6.4 mm (0.25 in) steel liner, it being in contact with the inside surface of the concrete. The dynamic load was applied over the whole circumference to a height of 2.5 m (8.2 ft). This is to conservatively envelope the two classes of lower pool depths defined above. The applied impulses were varied by adjusting the peak amplitude and time-duration of a triangular pressure pulse.

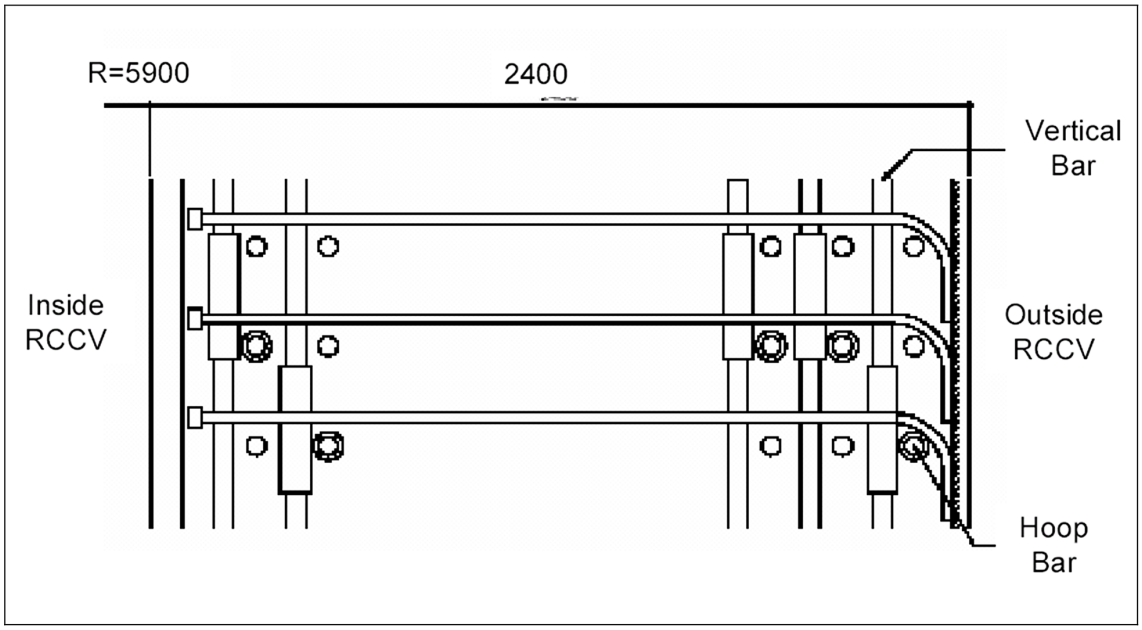

		Arrangement	Rebar ratio (%)
Hoop	Outside	3 - # 18 @ 300	1.08
	Inside	2 - # 18 @ 300	0.72
Vertical	Outside	3 - # 18 @ 1.8 ^{o}	1.51
	Inside	2 - # 18 @ 1.8 ^{o}	1.01
Shear		# 9 @ 300x300	0.72

Figure 21.4.4.4-1. Reactor Pedestal DYNA3D Model Structural Definition

Structural definition of the reactor pedestal (2.4 m thick) used in the DYNA3D model.

Three results selected around the condition of failure are shown in Figure 21.4.4.4-3. The peak pressures utilized in these calculation are in the 1.3 to 2 kbar (19,000 to 29,000 psi) range, and pulse widths were of 3 and 6 ms. At the low end, the impulse is ~200 kPa s (29 psi.s), and at the high end it is 600 kPa s (87 psi.s). The calculated strains show that at the upper end (600 kPa s, 87 psi.s) there is incipient liner failure. At the same time the concrete seems to have suffered sufficient damage that it can be considered near the end of its load-bearing capacity. On the other hand, the intermediate case — 2 kbar (29,000 psi) peak pressure, 3 ms pulse, 300 kPa.s (44 psi.s) impulse — is seen to hold up quite well, and so is the lowest impulse case at 200 kPa.s (29 psi.s). Further results testing the sensitivity to concrete model (an earlier version in the DYNA3D code), are summarized in Figures 21.4.4.4-4a through f. It is clear that there is a significant benefit from the improved model, and that the previous, general "understanding" that failure can be expected at ~100 kPa.s (14.5 psi.s), at least for the ESBWR, needs to be revised upwards to ~0.5 MPa.s (73 psi.s).

See also Addendum (21.4.7) to this Section at the end of Section 21.4.

The BiMAC device, Figure 21.4.2-2, was modeled conservatively in a quasi 1D fashion; that is, the load was assumed to be applied over the whole floor area, which allows vertical planes of symmetry through any two adjacent pipes (steel A36), and thus a great detail in the DYNA3D representation, as illustrated in Figure 21.4.4.4-5. Calculations were carried out with the same type of impulse loadings as done for the reactor pedestal. The results leading up to crushing of the pipes are shown in Figure 21.4.4.4-6. Note that at around 200 kPa.s (29 psi.s), a thin portion of the pipes yields significantly, however, the remaining material remains basically intact, while the pipe cross-sectional area is still largely intact. We take this as the level of incipient failure by crushing.

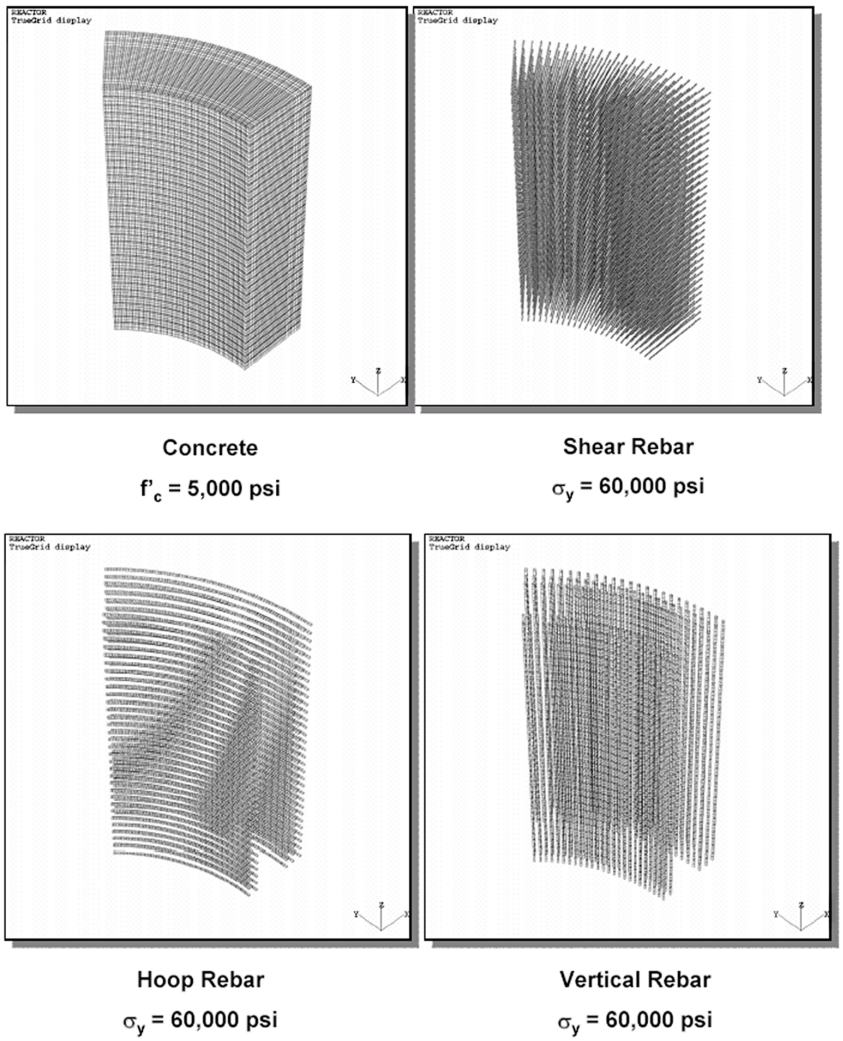

Figure 21.4.4.4-2. The DYNA3D Model Used in the Fragility Calculations

The DYNA3D model used in the fragility calculations. A 6-m vertical wall was azimuthally cut to a 450 segment by planes of symmetry as shown. The discretization involved 0.5 million hexahedral elements. Also shown are the radial (shear), hoop, and vertical rebar positions, all included in the model. Calculations were also run with the steel liner (6 mm) in place (not shown in figure).

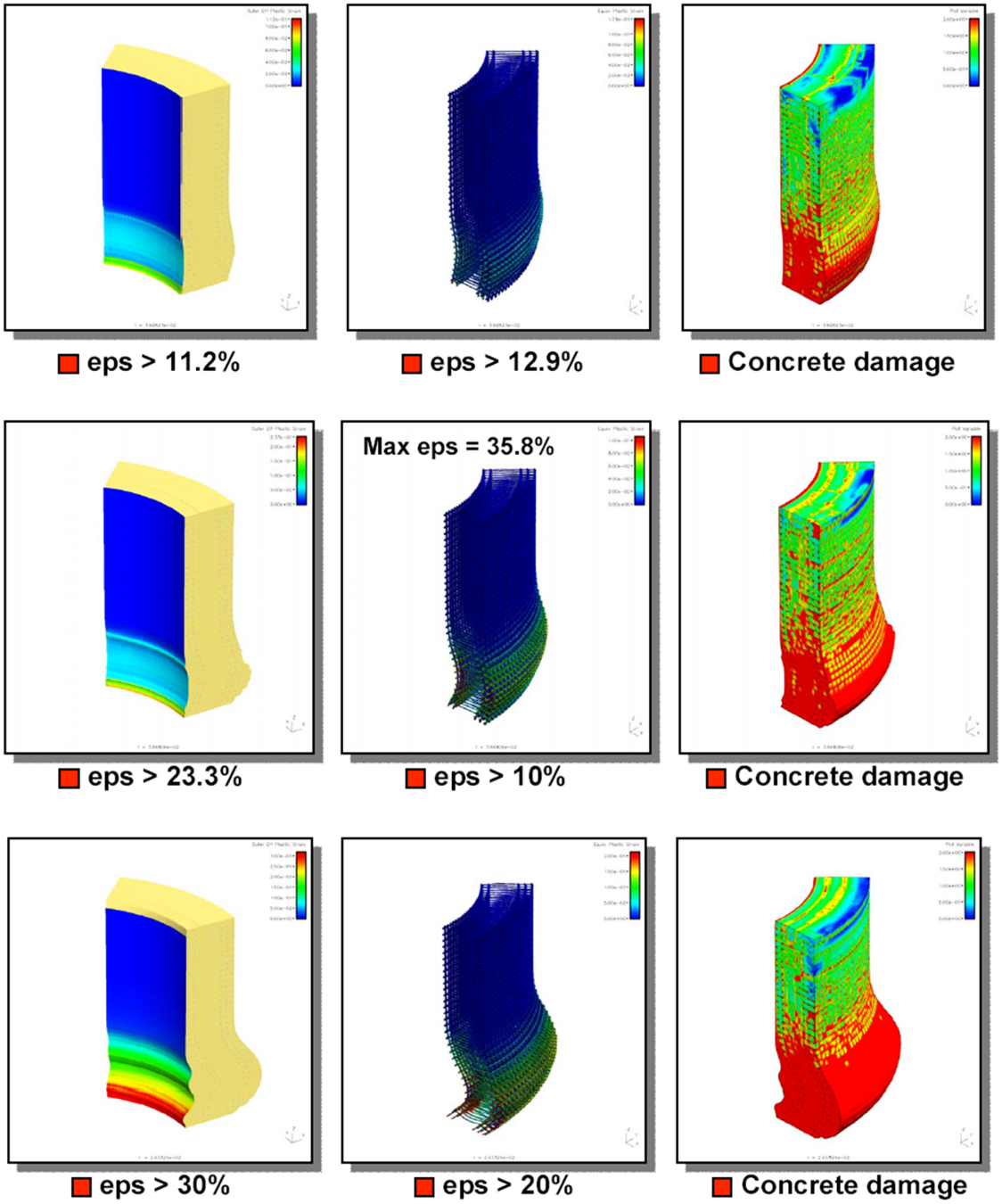

Figure 21.4.4.4-3. Results of Three Load Cases in DYNA3D

Results of three load cases in DYNA3D, with the new (improved) K&C concrete model. Top row 1.3 kbar, 3 ms pulse (195 kPa.s), middle row 2 kbar, 3 ms pulse (300 kPa.s), bottom row 2 kbar, 6 ms pulse (600 kPa.s). Left column: liner effective plastic strain. Central column: rebar strain. Right column: concrete damage.

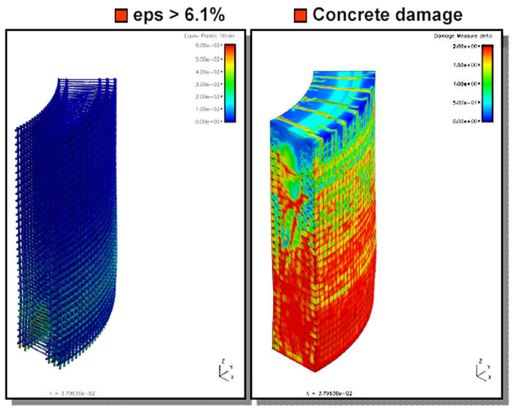

(a)

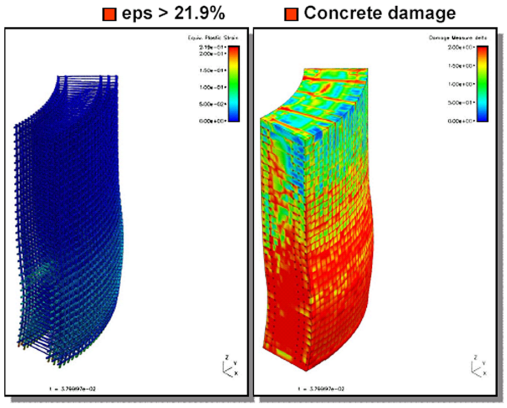

(b)

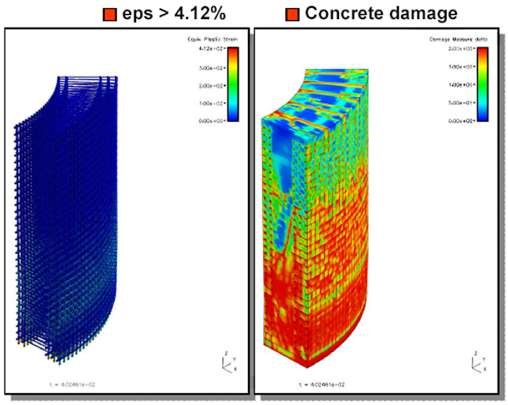

(c)

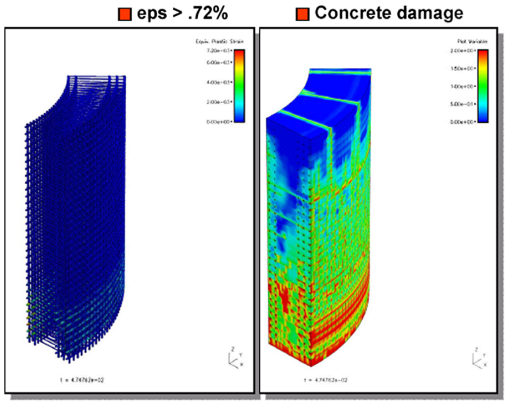

(d)

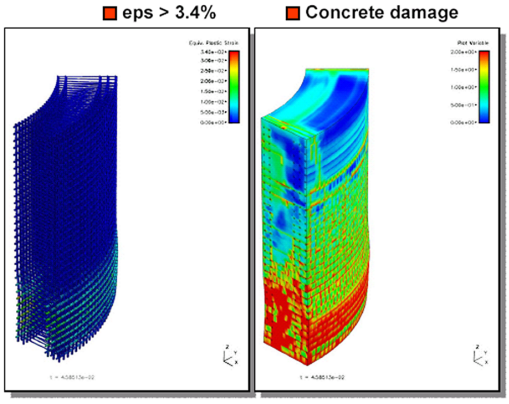

(e)

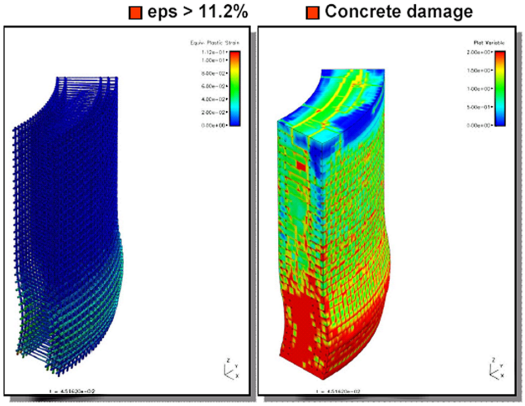

(f)

Figures 21.4.4.4-4. Results of Three Load Cases Calculated With Dyna3d Code

Results of three load cases, calculated with the standard (SKC) and improved K&C (IKC) concrete models in DYNA3D code.

(a) 0.33 kbar, 3 ms pulse (50 kPa.s) (SKC); (b) 0.65 kbar, 3 ms pulse (100 kPa.s) (SKC);

(c) 1.30 kbar, 3 ms pulse (195 kPa.s) (SKC); (d) 1.30 kbar, 3 ms pulse (195 kPa.s) (IKC);

(e) 1.30 kbar, 6 ms pulse (390 kPa.s) (IKC); (f) 0.65 kbar, 6 ms pulse (195 kPa.s) (IKC).

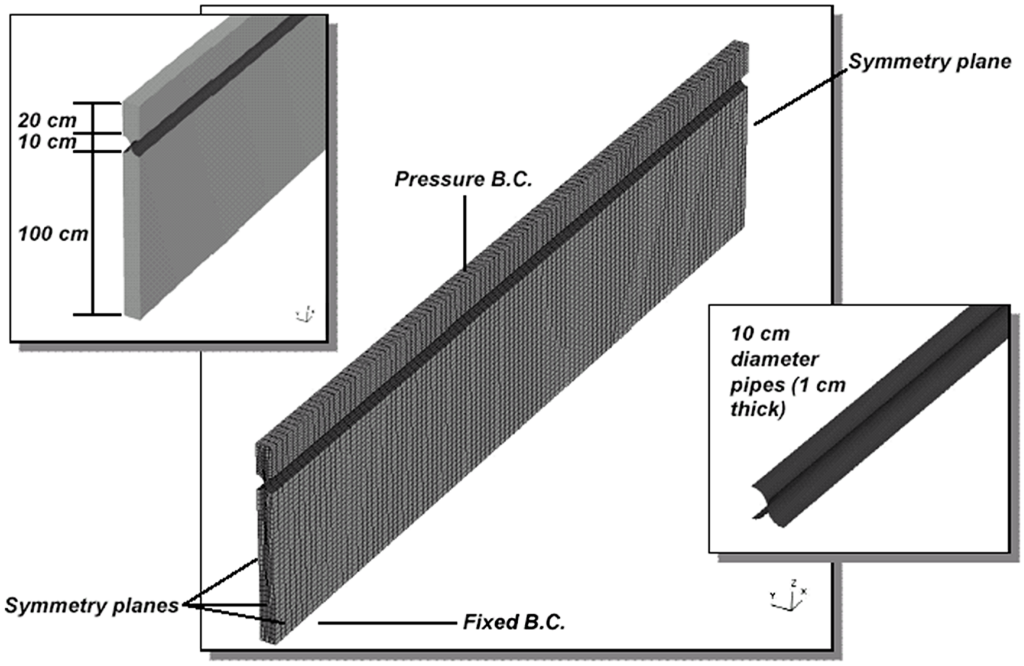

Figure 21.4.4.4-5. The Dyna3d Representation of the BiMac Device

The DYNA3D representation of the BiMAC device. There are 40,000 hexahedral elements and 2,000 shell elements (for the pipe material).

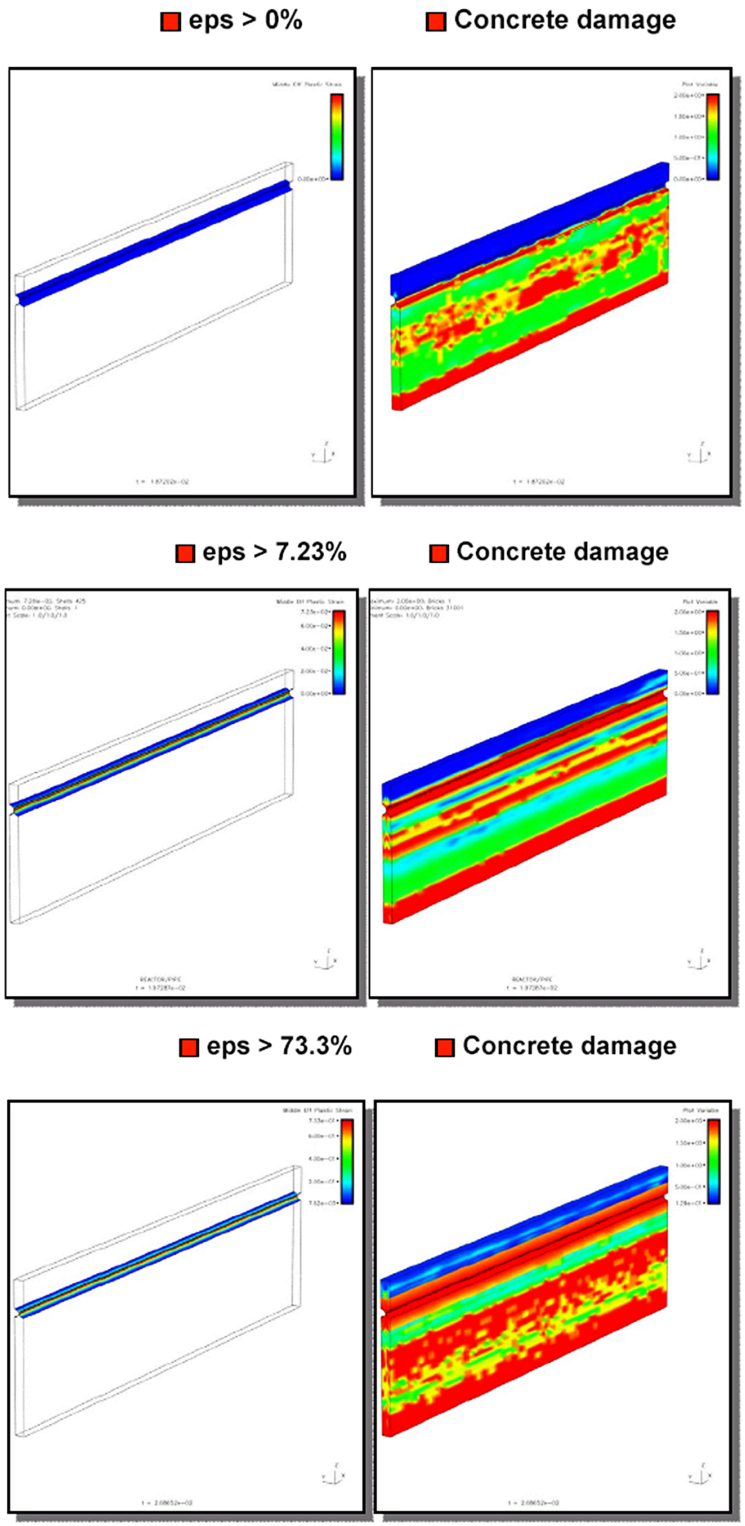

Figure 21.4.4.4-6. Extent of Concrete Damage Calculated By DYNA3D

Strain of the pipe, and extent of concrete damage calculated by DYNA3D. Top to bottom the impulses were 50, 100, and 200 kPa s respectively.

21.4.4.5 Prediction of Failure Probability

The results of the previous two sections on pedestal loads and fragility are juxtaposed in Figure 21.4.4.5-1. The loads from 1 and 2 m (3 and 6.5 ft) deep, highly sub-cooled pools are taken to bound loads from shallow, saturated pools. There is a huge margin in this bound, and as the figure shows there an extra huge margin to failure even given this bounding of loads. Thus we conclude that in 99% [90%] of the Class I severe accidents in ESBWR, pedestal failure by an EVE are physically unreasonable. This covers ~99% [~59%] of the CDF.

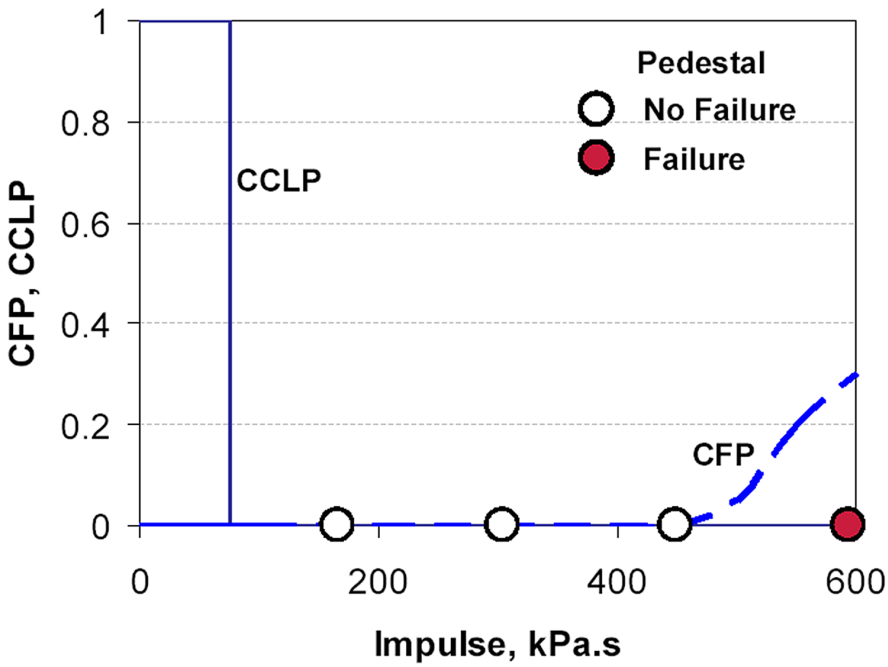

Figure 21.4.4.5-1. Failure and Load Probabilities for the Pedestal Cumulative Failure Probability (CFP) and Complementary Cumulative Load Probability (CCLP) for the pedestal.

The remaining 1% refers to Class I with deep (H >> 1.5 m (4.9 ft)) [10% of Class I], sub-cooled water pools. For such pools, although not considered in any detail here, an appropriately conservative position would be that "integrity of both the liner and the concrete structure could be possibly compromised."

Similarly the results for the structural integrity of the BiMAC can be visualized with the help of Figure 21.4.4.5-2. Failure incipience is shown at impulses of somewhere between 100 and 200 kPa.s (14.5 psi.s and 29 psi.s). Two load types are indicated. The realistic one is for the low level (LL) case, which would yield negligible energetics. The high level (HL) case is to schematically illustrate a bounding load appropriate for 1-2 meter (3-6.5 ft) deep, sub-cooled water pools that were analyzed. We can see that for 99% [90%] of the Class I severe accident scenarios BiMAC failure by an EVE would be physically unreasonable. We also see that BiMAC is structurally so strong as to allow significant margins to failure even in many EVEs postulated to occur in deeper and sub-cooled pools.

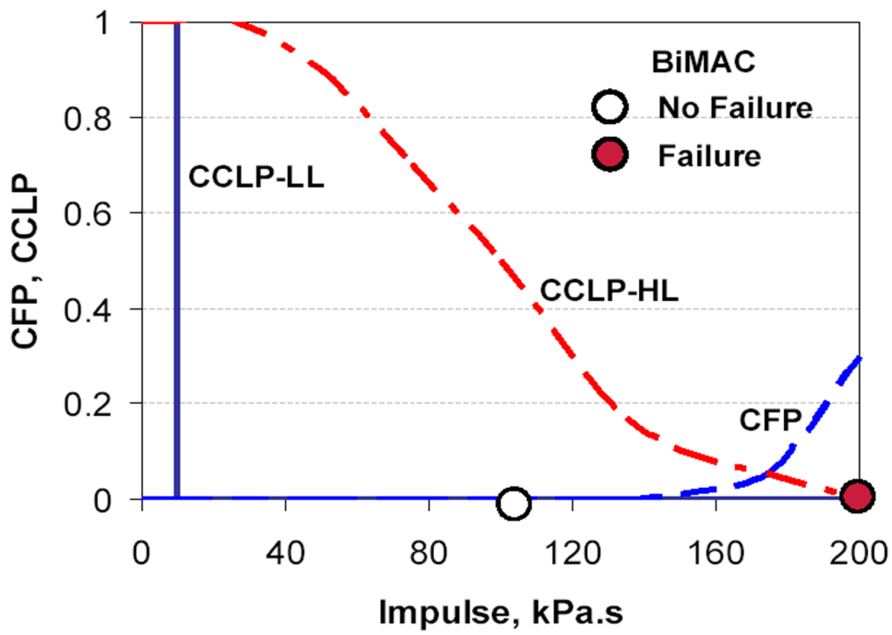

Figure 21.4.4.5-2. Failure and Load Probabilities for the Bimac Pipes

Cumulative Failure Probability (CFP) and Complementary Cumulative Load Probability (CCLP) for the BiMAC pipes for case with low water level (LL) and high water level (HL).

21.4.5 Summary and Conclusions for EVE

The above results show that for all but 1% [7%] of the CDF, that is accidents involving deep, subcooled water pools, violation of the ESBWR containment leak-tightness, and of the BiMAC function, due to ex-vessel steam explosions are physically unreasonable.

Principal ingredients to such a conclusion can be recapitulated as follows:

(1) An accident management strategy, and related hardware features that prohibit large amounts of cold water from entering the LDW prior to RPV breach,

(2) The physical fact that premixtures in saturated water pools become highly voided and thus unable to support the escalation of natural triggers to thermal detonations,

(3) Reactor pedestal and BiMAC structural designs that are capable of resisting explosion load impulses of over ~500 kPa s (73 psi.s) and ~100 kPa s (14.5 psi.s) respectively.

21.4.6 References

21.4.-1 Almström, H., Sundel, T., Frid, W., Engelbrektson, A. (1999), "Significance of fluid-structure interaction phenomena for containment response to ex-vessel steam explosions," Nuclear Engineering and Design, v.189, pp.405–422.

21.4.-2 Amarasooriya, W.H. and Theofanous, T.G. (1991), "Premixing of Steam Explosions: A Three-Fluid Model," Nuclear Engineering & Design 126, 23-39.

21.4.-3 DYNA3D (2004). Code Manual. Lawrence Livermore National Laboratory.

21.4.-4 GE (1987; 1994) General Electric. Standard Safety Analysis Report (SSAR) for ABWR (1994 Final Submission version).

21.4.-5 Henry, R.E. and Fauske, H.K. (1981), "Required Initial Conditions for Energetic Steam Explosion," ASME HTD v.19, pp.99-108.

21.4.-6 Esmaili, H. and Khatib-Rahbar, M. (2005), Analysis of likelihood of lower head failure and ex-vessel fuel coolant interaction energetics for AP1000. Nuclear Engineering and Design, 235 (15), July 2005, pp. 1583-1605.

21.4.-7 Fletcher, D.F. and Theofanous, T.G. (1997) "Heat Transfer and Fluid Dynamic Aspects of Explosive Melt-Water Interactions," Advances in Heat Transfer, 29, 129-213.

21.4.-8 Malvar, L.J., Crawford, J.E., Wesevich, J.W., Simons. D. (1997) "A Plasticity Concrete Material Model for DYNA3D." Int. J. Impact Engineering Vol. 19, Nos. 9-10, pp. 847-873, 1997.

21.4.-9 Noble, C.J. et al (2005). "Concrete Model Description and Summary of Benchmark Studies for Blast Effects and Simulation." UCRL-215024, Lawrence Livermore National Laboratory (July, 2005).

21.4.-10 NRC (1994). U.S. Nuclear Regulatory Commission. "Final safety evaluation report related to the certification of the advanced boiling water reactor design," NUREG-1503.

21.4.-11 NUREG–1150 (1990). Severe Accident Risks: An assessment for five U.S. nuclear power plants. Technical Report NUREG–1150, U.S. Nuclear Regulatory Commission.

21.4.-12 Rashid, Y.R., Theofanous, T.G., and Foadian, H. (1995), Failure Assessment of Reactor Vessel Support Structure Subjected to Ex-Vessel Explosion Loads, 1995 ASME/JSME Pressure Vessel and Piping Conference, Honolulu, Hawaii, July23-27, 1995. Also published in a Trans. of the ASME, Journal of Pressure Vessel Technology (1997).

21.4.-13 SERG (1985) Review of the current understanding of the potential for containment failure from in-vessel steam explosions, NUREG-1116, U.S. NRC (1985).

21.4.-14 SERG-2 (1995) Proceedings of the Second Steam Explosion Review Group (SERG-2) Workshop, NUREG-1524, ed., S. Basu and T. Ginsberg, August 1996. (Follow-on international FCI research summarized in Proceedings of the OECD/CSNI Specialists Meeting on Fuel-Coolant Interactions, NEA/CSNI/R(97)26, ed., M. Akiyama, N. Yamano and J. Sugimoto, January 1998).

21.4.-15 Theofanous, T.G., Najafi, B., and Rumble, E. (1987), "An Assessment of Steam-Explosion-Induced Containment Failure. Part I: Probabilistic Aspects," Nuclear Science and Engineering, 97, 259-281 (1987). M.A. Abolfadl and T.G. Theofanous, "An Assessment of Steam-Explosion-Induced Containment Failure. Part II: Premixing Limits," Nuclear Science and Engineering, 97, 282-295 (1987). W. H. Amarasooriya and T.G. Theofanous, "An Assessment of Steam-Explosion-Induced Containment Failure. Part III: Expansion and Energy Partition," Nuclear Science and Engineering, 97, 296-315 (1987). G.E. Lucas, W.H. Amarasooriya and T.G. Theofanous, "An Assessment of Steam-Explosion-Induced Containment Failure. Part IV: Impact Mechanics, Dissipation and Vessel Head Failure," Nuclear Science and Engineering, 97, 316-326 (1987).

21.4.-16 Theofanous, T.G. (1995) "The Study of Steam Explosions in Nuclear Systems," Nuclear Engineering & Design 155 (1995) 1–26. (Also see S. Angelini, E. Takara, W.W. Yuen and T.G. Theofanous, "Multiphase Transients in the Premixing of Steam Explosions," Nuclear Engineering & Design, 146, 83-95, 1994. W.W. Yuen, X. Chen and T.G. Theofanous, "On the Fundamental Microinteractions That Support the Propagation of Steam Explosions," Nuclear Engineering & Design, 146, 133-146, 1994).

21.4.-17 Theofanous, T.G., and Yuen, W.W. (1995) "The Probability of Alpha-Mode Containment Failure Updated," Nuclear Engineering & Design 155 (1995) 459–473.

21.4.-18 Theofanous, T.G., Yuen, W.W., Zhao, H., Jansson, I., Frid, W. (1995). A study of ex-vessel steam explosions in Swedish BWRs. Proc. OECD Specialist Meeting on Selected Containment Severe Accident Management Strategies, Stockholm, Sweden, 13–15 June 1994, SKI Report 95:34, NEA:CSNI:R(95)3.

21.4.-19 Theofanous, T.G. (1996), "On the Proper Formulation of Safety Goals and Assessment of Safety Margins for Rare and High-Consequence Hazards," Reliability Engineering & Systems Safety, 54 (1996) 243–257.

21.4.-20 Theofanous, T.G., Yuen, W.W., and Angelini, S. (1999a), "The Verification Basis of the PM-ALPHA Code," Nuclear Engineering & Design, 189 (1999) 59-102. (Also T.G. Theofanous, W.W. Yuen and S. Angelini, "Premixing of Steam Explosions: PM-ALPHA Verification Studies," DOE/ID-10504, June 1998.)

21.4.-21 Theofanous, T.G., Yuen, W.W., Freeman, K. and Chen, X. (1999b), "The Verification Basis of the ESPROSE.m Code," Nuclear Engineering & Design, 189 (1999) 103-138. (Also T.G. Theofanous, W.W. Yuen, K. Freeman and X. Chen, "Propagation of Steam Explosions: ESPROSE.m Verification Studies," DOE/ID-10503, June 1998).

21.4.-22 Theofanous, T.G., Yuen, W.W., Angelini, S., Sienicki, J.J., Freeman, K., Chen, X. and Salmassi, T. (1999c) "Lower Head Integrity Under Steam Explosion Loads," Nuclear Engineering & Design, 189 (1999) 7-57. (Also T.G. Theofanous, W.W. Yuen, S. Angelini.)

21.4.-23 J.J. Sienicki, K. Freeman, X. Chen and T. Salmassi, "Lower Head Integrity Under In-Vessel Steam Explosion Loads,"DOE/ID-10541, June 1998.)

21.4.-24 Turland, B.D., Fletcher, D.F., and Hodges, K.I. (1994), "Quantification of the Probability and Containment Failure Caused by an In-Vessel Steam Explosion for the Sizewell B PWR," NUREG/CP-0127, 1994.

21.4.-25 Westinghouse Electric Company (2002). The AP1000 Design Control Document.

21.4.-26 Yuen, W.W. and Theofanous, T.G. (1995) "ESPROSE.m: A Computer Code for Addressing the Escalation/Propagation of Steam Explosions," DOE/ID-10501, April 1995.

21.4.-27 Yuen, W.W. and Theofanous, T.G. (1995) "PM-ALPHA: A Computer Code for Addressing the Premixing of Steam Explosions," DOE/ID-10502, May 1995.

21.4.-28 Yuen, W.W. and Theofanous, T.G. (1995) "The Prediction of 2D Thermal Detonations and Resulting Damage Potential," Nuclear Engineering & Design, 155 (1995) 289-309.

21.4.-29 Yuen, W.W. and Theofanous, T.G. (1999) "On the Existence of Multiphase Thermal Detonations," Int. Jl. Multiphase Flow, 25 (1999) 1505-1519.

21.4.-30 Noble, C. R., "DYNA3D Finite Element Analysis of Steam Explosion Loads on a Pedestal Wall Design," UCRL-TR-227386, January 22, 2007.

21.4.7 Quantification of Fragility (Addendum of Dec. 19, 2006)

This Addendum is to respond to reviewer's request for more legible structural analyses figures. Enlarged figures and a more detailed discussion of the structural analysis calculations can be found in Reference 21.4-30 This reference includes additional calculations performed with material (rebar) properties used in one of the reviewer's calculations. These are presented along with additional comments on fragility of the pedestal under ROAAM Review correspondence with Dr. J Rashid in Reference 21.2-18.